SIMULATION WITH THE DIONISIO 1.0 CODE OF THE OPERATION BEHAVIOR OF PWR/PHWR FUEL RODS

Alejandro Soba, Alicia Denis

Departamento Combustibles Nucleares, Comisión Nacional de Energía Atómica,
Avenida del Libertador 8250, 1429 Buenos Aires, Argentina

Key words: DIONISIO Code, IAEA DATABASE, fuel performance, contact model.

Abstract

We summarize the present status of the code DIONISIO 1.0 that describes most of the main phenomena occurring in a PWR/PHWR fuel rod throughout its life under normal operation conditions. Two calculation scenarios are permitted: system constituted by pellet and cladding, assuming a closed gap from the beginning of life, or constituted by pellet, gap and cladding, where the possibility of gap closure and reopening during burnup is allowed.

Starting from an idealized power history, the code predicts the temperature distribution in the domain, elastic and plastic stress and strain, creep, swelling and densification, release of fission gases, cesium and iodine to the internal free volume of the rod, gas mixing, pressure increase, irradiation growth of the Zircaloy cladding, development of an oxide layer on its surface and hydrogen uptake, restructuring and grain growth in the pellet. The effects of an internal or external corrosive atmosphere (SCC) as well as the possibility of pellet-cladding interaction (PCI) are also considered.

The code is two-dimensional, assumes cylindrical symmetry for the rod and uses the finite element method to integrate the differential equations, some of which are non-linear. The diverse models are interconnected and mutually dependent.

In the present occasion, results corresponding to PHWR reactors are presented. Good results are obtained for the simulation of irradiation tests contained in IAEA databases: IFPE/AECL-BUNDLE, performed in the NRU experimental reactor at the Chalk River Laboratories; the CONTACT series of experiments performed in the Siloe Reactor, Grenoble, designated IFPE/CONTACT REV.1; the irradiation tests EFE N51 and EFE N89 performed in the Nuclear Research Institute Pitesti, Romania, and several experiments selected from the FUMEX II cases.

1. Introduction

The DIONISIO code performs the calculations in a domain representing the pellet, the gap and the cladding. Cylindrical symmetry around the longitudinal axis as well as symmetry with respect to the middle transversal plane are assumed. The scheme of Figure 1 represents the *r-z* domain used for the simulations.

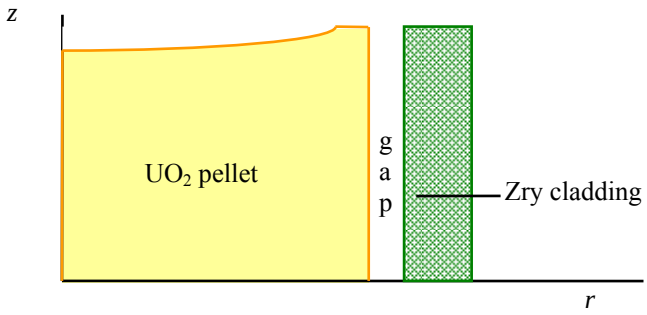

Figure 1*: Pellet-gap-cladding system analyzed in DIONISIO*

The strain analysis of the pellet and the cladding considers the elastic and plastic regimes and includes thermal expansion, swelling, densification, creep and irradiation growth of the cladding for sufficiently long periods [1]. Due to thermal expansion and to the mechanical restrictions of the pellet, it experiences a non-uniform deformation: the initially cylindrical pellet surface distorts, bending outwards, the top and bottom faces being displaced further than the central belt [2]. If the pellet strain is sufficiently large, it may come into contact with the cladding (PMCI), particularly in regions next to the pellet-pellet contact surfaces.

The fission products of gas nature, mainly Xe and Kr, due to the low solubility in the oxide lattice, form intra and intergranular bubbles. The latter accumulate gas until they reach a saturation level. After that, the gas in excess is released to the plenum, the gap and the dishing. In this manner, it contributes to increasing the internal pressure in the fuel rod, modifies the gap thickness and decreases the thermal conductance of the gap, which is reflected in a further temperature increase. The fission gas inventory is obtained as the solution of the diffusion equation of gas in a spherical grain of UO_2 [3,4].

The fission products, either solid or gaseous, dissolved in the oxide matrix and both types of gas bubbles occupy a volume larger than that of the original material and produce pellet swelling, obeying to different laws according to the case.

The high temperature and thermal gradient in the fuel also generate grain growth and pore migration towards the pellet center. The consequent fuel restructuring is evidenced by the presence, at the end of life, of radial zones with different grain size and morphology: columnar grains at the center, large equiaxed grains in the middle zone, and fine as-fabricated grains at the external pellet ring. Besides that, radial and axial fuel cracks develop in the pellet with the effect of making it appear as constituted of a softer material.

The code presented here takes account of these phenomena. It solves first the heat diffusion equation taking as input data the power history and the boundary conditions: constant temperature at the external surface of the fuel element and temperature gradient equal zero at

the pellet center line. The temperature distribution in the pellet, the gap and the cladding is thus obtained. To this end, a finite element scheme in cylindrical coordinates is used. The temperature dependence of the oxide thermal conductivity is responsible for the non-linearity of the thermal problem. This imposes the need of an iterative procedure to calculate the temperature at each node. With the same discretization and with the results of the thermal step, the stress-strain problem is solved. Plasticity and creep render this calculation also non-linear.

The code also calculates pore migration, grain growth and differential restructuring in the fuel, the amount of fission products in the internal atmosphere, hydrogen uptake by the cladding, which contribute to the strain hardening, and oxide growth on the external cladding surface, responsible for the modification of the boundary condition of the thermal problem.

2. General Models

2.1 The thermal problem

The temperature distribution in each rod material is obtained by solving the differential equation in cylindrical coordinates

$$\frac{1}{r}\frac{\partial}{\partial r}\left(r\, k_r^j(T)\frac{\partial T}{\partial r}\right)+\frac{\partial}{\partial z}\left(k_z^j(T)\frac{\partial T}{\partial z}\right)=-Q^j(r)$$

where $T(r,z)$ represents the temperature, $k^j(T)$ is the thermal conductivity of material j in the r and z direction and Q^j is the volumetric heat generation rate given by

$$Q^j=\begin{cases} Q^f & \text{in the } UO_2 \text{ fuel pellet} \\ 0 & \text{other material} \end{cases}$$

Q^f changes with time according to the power history. The boundary conditions are

$$\left.\frac{\partial T}{\partial r}\right|_{r=0}=0 \;\;;\;\; h_{fc}\left[T(r_{ef})-T(r_{ic})\right]=\frac{P_l(z)}{2\pi r_{ef}} \;\;;\;\; k^c(T)\left.\frac{\partial T}{\partial r}\right|_{r=r_{ic}}=-\frac{P_l(z)}{2\pi r_{ic}} \;\;;\;\; T(r_{ec})=T_C(z)$$

where $P_l(z)=\pi\, r_{ef}^2\, Q^f(z)$ is the lineal power, r_{ef}, r_{ic} and r_{ec} are the external and internal radii of the fuel and the cladding. The external cladding temperature $T_C(z)$ is calculated in terms of the coolant temperature $T_R(z)$, the thermal jump at the tube-coolant interface and the temperature variation through the cladding oxide layer [5,6]. h_{fc} is the thermal conductance of the gap between the fuel and cladding surfaces; it contains the contributions of three terms $h_{fc}=h_{rad}+h_{gas}+h_s$: h_{rad} is due to radiation effects; h_{gas} depends on the composition of the gap atmosphere; the term h_s represents the contribution of the solid portions of surface in contact and hence is different to zero when the gap is partially or totally close

DIONISIO also allows selecting a pellet with a central hole. In this situation, a new equation for this medium is needed with a thermal conductivity of a gas mixing type and null power generation.

2.2. The stress-strain analysis

Given the axial symmetry of the system, neither the geometry nor the surface loadings depend on the angular coordinate. The displacements, strains and stresses are functions of *r* and *z* only. If *u* and *w* represent the displacements in the *r* and *z* directions, respectively, the strain-displacement relations are [7]:

$$e_{rr} = \frac{\partial u}{\partial r} \quad ; \quad e_{\theta\theta} = \frac{u}{r} \quad ; \quad e_{zz} = \frac{\partial w}{\partial z} \quad ; \quad e_{rz} = \frac{\partial u}{\partial z} + \frac{\partial w}{\partial r} \quad ; \quad e_{r\theta} = 0 \quad ; \quad e_{z\theta} = 0 \qquad (1)$$

The column vector $\{e\}$ contains the non-zero components of the strain:

$$\{e\}^T = [e_{rr} \quad e_{\theta\theta} \quad e_{zz} \quad e_{rz}]$$

The superscript *T* indicates the transpose. $\{e\}$ has different contributions depending on the material. For the cladding, it is given by

$$\{e\}^{clad} = \{\varepsilon_{th}\} + \{\varepsilon_{el}\} + \{\varepsilon_p\} + \{\varepsilon_c\} + \{\varepsilon_i\}$$

where the terms stand for the (*th*) thermal, (*el*) elastic, (*p*) plastic, (*c*) creep and (*i*) irradiation growth strains, respectively. For the pellet, it is

$$\{e\}^{pellet} = \{\varepsilon_{th}\} + \{\varepsilon_{el}\} + \{\varepsilon_p\} + \{\varepsilon_c\} + \{\varepsilon_{sw}\} + \{\varepsilon_d\}$$

with a similar meaning of the terms, except for the inclusion of the swelling $\{\varepsilon_{sw}\}$ and densification $\{\varepsilon_d\}$ contributions.

The thermal strain is defined as:

$$\{\varepsilon_{th}\}^T = [\alpha \Delta T \quad \alpha \Delta T \quad \alpha \Delta T \quad 0]$$

where α is the thermal expansion coefficient of the material. Swelling and densification (in the fuel material) also give origin to strain vectors without shear component. Three phenomena contribute to swelling: intragranular and grain boundary bubbles and lattice fission products. Then

$$\{\varepsilon_{sw}\} + \{\varepsilon_d\} = \frac{1}{3} \left. \frac{\Delta V}{V} \right|_{\text{int.bub.}} + \left. \frac{\Delta V}{V} \right|_{\text{g.b.bub.}} + \left. \frac{\Delta V}{V} \right|_{\text{l.f.p.}} + \left. \frac{\Delta V}{V} \right|_{\text{dens.}}$$

The elastic strain and the stress are related by the Hooke´s law

$$\{\sigma\} = [D]\{\varepsilon_{el}\}$$

The non-zero components of the stress are:

$$\{\sigma\}^T = [\sigma_{rr} \quad \sigma_{\theta\theta} \quad \sigma_{zz} \quad \sigma_{rz}]$$

[*D*] is the material matrix. Its elements are expressed in terms of the Young´s modulus and the Poisson´s ratio.

The values adopted for the materials constants are listed in *TABLE I*.

TABLE I. Material properties used in the code.

Young's modulus E (Pa) [8,9]	UO_2:	$2.065\times10^{11}\ (1+1.091\times10^{-4}\ T)$
	Zry :	$1.236\times10^{11} - 6.221\times10^{7}\ T$
Poisson's ratio μ [10]	UO_2:	$1.045 - 1.7025\ T+0.9265\ T^2$
	Zry:	0.32
Thermal expansion α (K^{-1}) [9]	UO_2:	$(-4.972\times10^{-4} + 7.107\times10^{-6}\ T + 2.583\times10^{-9}\ T^2\ )/\Delta T$
	Zry:	$(- 2.07\times10^{-3} + 6.72\times10^{-6}\ T)/\Delta T$
Thermal conductivity k ($Wm^{-1}K^{-1}$) [11,12]	UO_2:	$k^{pellet}(T) = \frac{1}{0.03494 + 2.243x10^{-4}T} + \frac{6.157x10^{9}}{T^2}\exp\left[-\frac{1.41x1.6x10^{-19}}{kT}\right]$
	Zry:	$k^{clad}(T) = 7.51 + 2.09\times10^{-2}T - 1.45\times10^{-5}T^2 + 7.67\times10^{-9}T^3$
	Gap:	gas mixture model
Yield stress σ_Y (Pa) [10]	UO_2:	$108000\times10^{-T/1225}$
	Zry:	$6.578\times10^{4}(1 - 1.686\times10^{-3}T + 7.748\times10^{-7}T^2$

The plastic term is obtained by a recursive procedure in which the values of stress and strain are fitted to the uniaxial curve corresponding to the material involved. In the temperature range involved in nuclear fuel normal performance only the Zry exhibits a significant plastic deformation.

The model of fuel creep adopted [8] assumes that the creep rate depends on the power regime: constant or ramp [13]. Depending on the stress state, the pellet creep rate law can be linear or proportional to the stress. The transition stress in Pa is given by the empirical relation $\sigma_t = \frac{1.6547\times10^{7}}{G^{0.5714}}$, where G is the grain size in μm.

For the Zircaloy cladding the creep model included in DIONISIO was taken from ref. [14] and that for irradiation growth model from ref. [15]. In *Table II* the models used are listed.

When the finite element method is applied, the unknown displacements u and w are written in terms of the element nodal values and the shape functions. The differential equations (1) are thus transformed to linear equations, which are formally similar to those for the thermal problem.

Table II. Models used in DIONISIO

Creep rate law for UO_2 (s^{-1}) [8] a_1-a_8 constants; $\dot{f}$ fission density; σ applied stress, G grain size, Q_1, Q_2 y Q_3 activation energies.	$\dot{\varepsilon} = \frac{(a_1 + a_2\dot{f})\sigma \exp(-Q_1/RT)}{(a_3 + D)g^2} + \frac{(a_4 + a_8\dot{f})\sigma^{4.5}\exp(Q_2/RT)}{a_6 + D}$ $+ a_7 * \sigma\dot{f}\exp(Q_3/RT)$
Creep rate law for Zry (s^{-1}) [14] k, b and c are constants, ε_{eq} generalized fluence strain	$\varepsilon = f(\sigma, T, t, \dot{f}) = \frac{(2a_1a_2a_3)^2}{\varepsilon_{eq}}$; $a_1 = k\dot{f}$; $a_2 = \exp\left(-\frac{10000}{RT}\right)$; $a_3 = \sigma_{Hoop} + b\exp(c\sigma_{Hoop})$
Cladding irradiation growth [15] ϕ = fast neutrons flux (n/cm^2 s)	$d\varepsilon_{zz}^{Ig}/dt = 4.942x10^{-20}\phi$ $d\varepsilon_{rr}^{Ig}/dt = -0.941\, d\varepsilon_{zz}^{Ig}/dt$ $d\varepsilon_{\theta\theta}^{Ig}/dt = -0.059\, d\varepsilon_{zz}^{Ig}/dt$
Swelling due to intragranular bubbles [3,4] C_B concentration of intragranular bubbles; R_B bubbles radius	$\left.\frac{\Delta V}{V}\right\|_{\text{int.bub.}} = \frac{(4/3)\pi R_B^3 C_B}{1-(4/3)\pi R_B^3 C_B} \approx (4/3)\pi R_B^3 C_B$
Swelling due to intergranular bubbles[3,4] P_{ext}, external pressure $2\gamma/r_f$ stress due to surface tension; r_f radius of curvature of the bubble's face; N surface concentration of gas atoms; k Boltzmann constant	$\left.\frac{\Delta V}{V}\right\|_{\text{g.b.bub}} = \frac{3kTN}{G(2\gamma/r_f + P_{ext})}$
Swelling due fission products in the fuel lattice [3,4]	$\left.\frac{\Delta V}{V}\right\|_{\text{l.f.p.}} = 0.0032\text{Bup[at\%]}$
Densification [3,4] b rate of bubbles resolution; P_0 initial porosity	$\left.\frac{\Delta V}{V}\right\|_{\text{dens.}} = -\frac{P_o(1-e^{-bt})}{1-P_o e^{-bt}} \approx -P_o(1-e^{-bt})$

temperatures T in K.

3. PCMI in DIONSIO

3.1 Thermal contact.

During reactor operation the gas composition in the gap varies because of the release of gaseous fission products. Due to the low conductivity of these gases, they contribute to temperature increase in the rod. At the same time, the gases accumulated in the gap increase the internal pressure of the rod.

The unequal mechanical response of the fuel and cladding materials during irradiation determines fluctuations in the gap width. It may remain open during most of the irradiation

history or it may close at the beginning of the irradiation and remain in that condition up to the end or it may be alternately open and closed. When pellet-cladding contact occurs, the thermal transfer depends on the roughness of both surfaces. The thermal conductance model included in DIONISIO takes into account all these facts [16]. A general review of the known models for the thermal gap conductance between UO_2 and Zry for both, open and closed gap, is found ref. [17].

Open gap: The gas atmosphere in the gap, assumed to be initially constituted by He only, modifies its composition during burnup due to the incorporation of fission gases, mainly Xe and Kr. Heat conduction through the gas mixture filling the pellet-cladding gap is the dominant mechanism of transfer. The gas conductivity is given by functions like [9,18]

$$k_i = A_i T^{B_i}$$

where A_i and B_i are constants and i = He, Xe, Kr, other. The gas composition is then a time function. The conductivity of the mixture is calculated in DIONISIO as [8]:

$$k_{gasmix} = \sum_{i=1}^{n} \beta_i x_i$$

with

$$\beta_i = k_i \left[x_i + \sum_{\substack{j=1 \\ j \neq i}}^{n} \psi_{ij} x_j \right]^{-1}$$

$$\psi_{ij} = \phi_{ij} \left[1 + 2.41 \frac{(M_i - M_j)(M_i - 0.142 M_j)}{(M_i + M_j)^2} \right]$$

$$\phi_{ij} = 2^{-3/2} \left(1 + \frac{M_i}{M_j} \right)^{-1/2} \left(1 + \left(\frac{k_i}{k_j} \right)^{1/2} \left(\frac{M_i}{M_j} \right)^{1/4} \right)^2$$

where M_i and x_i are the molecular weight and fraction of species i and i = He, Xe, Kr, other.

If the gap is wider than the mean free path of the gas molecules, the conductance of the gas phase in the gap is given by the simple formula:

$$h_{gas} = \frac{k_{gasmix}}{A_{gap}(t)}$$

where $A_{gap}(t)$ is the time dependent gap width.

When the fuel and cladding surfaces are closer than a few mean free paths of the filling gas molecules, the gas temperature immediately adjacent to each surface is not the same as the surface temperature since a thermal jump appears on each wall that modifies the conductance of the medium

Several authors propose a variety of models for the conductance between near surfaces [8,9,19,20]. The following expression was adopted in DIONISIO valid for a gap width similar to the mean roughness of both surfaces [8]

$$h_{gas} = \sum_{i=1}^{n} \beta_i x_i \left(A_{gap}(t) + \frac{4}{\hat{\alpha}_i P} \left(\frac{\gamma_i - 1}{\gamma_i + 1} \right) \sqrt{\frac{\pi M_i T_{gas}}{2R}} \; \beta_i \right)^{-1}$$

where h_{gas} is in W cm^{-2} K^{-1}, T_{gas} and P are the temperature and internal pressure in the gap measured in K and Pa, respectively, the subscript i indicates the gases that compose the mixture, γ_i is the ratio of the specific heat coefficients at constant pressure and constant volume, M_i is the molecular weight of gas i and $\hat{\alpha}_i$ is the effective thermal accommodation coefficient of component i; it involves the individual accommodation coefficients between each solid surface and the gas phase in between.

Radiation contribution: When the gap is open and the temperature is over 300^{o}C, it is necessary to consider the contribution of the radiation of each surface. An expression for this term is provided by Olander [9]

$$h_{rad} = \frac{4\lambda T^3}{(1/\varepsilon_c) + (1/\varepsilon_f) - 1}$$

where ε_j is the emissivity factor of each surface, T is the average between the external temperature of the fuel and the internal temperature of the cladding, λ=5.67x10^{-8} W m^{-2} K^{-4} is the Stefan-Boltzmann's constant. The values of emissivity adopted are [20]

$$\varepsilon_c = 0.1906 - 0.2166 \exp\left(-3.792 \times 10^{-3} T\right)$$
$$\varepsilon_f = 0.85$$

with T in the range (373-1900)K. For small gaps, the radiation influence is negligible as compared to that of conduction.

Closed gap: When the rough pellet and cladding surfaces are in contact, heat transport occurs partly by solid conduction in the area of physical contact and by gas conduction in the remaining area. The fraction of the surface area in contact depends on the way the deformation is produced (elastic or plastic), the compression stress, the internal pressure and the roughness of each surface.

Different works analyze the contact conductance. That included in DIONISIO [21] approximate the contact layer thickness δ as the mean square value of roughness of both solids (~4.4x10^{-6} m). This model improves if the contact radius is assumed to obey a pseudo-uniform distribution, i.e., the area surrounding the contact is proportional to its size, if the heights of the contact spots are assumed to follow a Gauss distribution. With these hypotheses, the expression for the contact conductance is:

$$h_s = 1.45\left(\frac{2k_f k_c}{k_f + k_c}\right)\left(\frac{P_i}{H}\right)^n \frac{\sqrt{(\tan\theta_f)^2 + (\tan\theta_c)^2}}{\sqrt{\delta_f^2 + \delta_c^2}}$$

where n=0.5 or 1 for elastic or plastic flow, $\tan\theta_i = \frac{2\delta_i}{\lambda_i}$ represents the average roughness slope of surface i and λ_i is the spacing between neighboring crests, assumed regular for an ideal surface.

3.2 Mechanical contact

The numerical treatment of PCMI in DIONISIO involves an algorithm based on Lagrange multipliers employing an irreducible formulation in each domain. The contact forces between the surfaces are derived from the virtual works principle, assuming continuity for the displacements at the boundaries and imposing restrictions to avoid interpenetration of the surfaces [22,23,24]. Starting from the applied external forces, the strain field is evaluated [25,26]. Its magnitude allows deciding if the surfaces come into contact or not. Different contact conditions are considered: sticking contact (without friction), sliding contact (with friction), repeated contact and separation between bodies. Where the contact is produced, the basic condition of no overlap between the surfaces gives origin to contact forces that act on both bodies, of equal magnitude and opposite sense. The only possible effect of the normal components is compression. In contrast, the tangential components can produce sliding depending on the relative magnitudes of both components. According to the Coulomb´s friction law, if there is no relative motion between the bodies when the contact is reached, no sliding takes place as long as the quotient tangential/normal components is lower than the static friction coefficient. If this limit is exceeded, sliding occurs. During motion, the magnitude of the tangential traction resisted by friction is governed by the dynamic friction coefficient.

When the stress distribution of both surfaces is such that overlap between them had to occur, the contact subroutine performs a number of iterations until overlap is eliminated and the deformed surfaces are in contact. (In the FEM formulation the contact condition is met when a boundary node of the source overlaps with a receptor segment, limited by two nodes). Starting from the stiffness and contact matrices and the nodal, external and contact force vectors at a given iteration, an incremental procedure is used [16,26] that gives the new values of the displacement vector, the normal and tangential stress in each node and the components of the contact forces for the following iteration. This leads to the condition of sticking or sliding contact of surfaces, or separation [24,25]. The number of equations to be solved depends on which condition is met.

4. Code testing

FUMEX cases

DIONISIO was used to simulate the experiments performed within the FUMEX 1 exercise. As an example of the results obtained, Figure 5 shows the comparison between the

experimental data and the predictions of the several codes that participated in the exercise [27]. The results obtained with DIONISIO are in general in good agreement with the experiments.

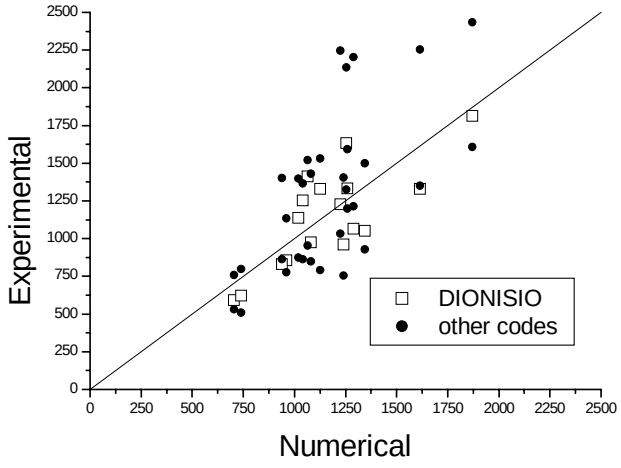

Figure 5: Comparison between the FUMEX 1 experimental data and the numerical results obtained with DIONISIO and other codes for the centre rod temperature.

Experiments with MOX fuels

One of the sets of experimental data used to compare the code results with comes from the irradiation of the first argentine prototypes of MOX fuels for PHWR reactors [28].The experimental data proceed from the rods identified as A.1.2 and A.1.3 which were subjected to different power histories.

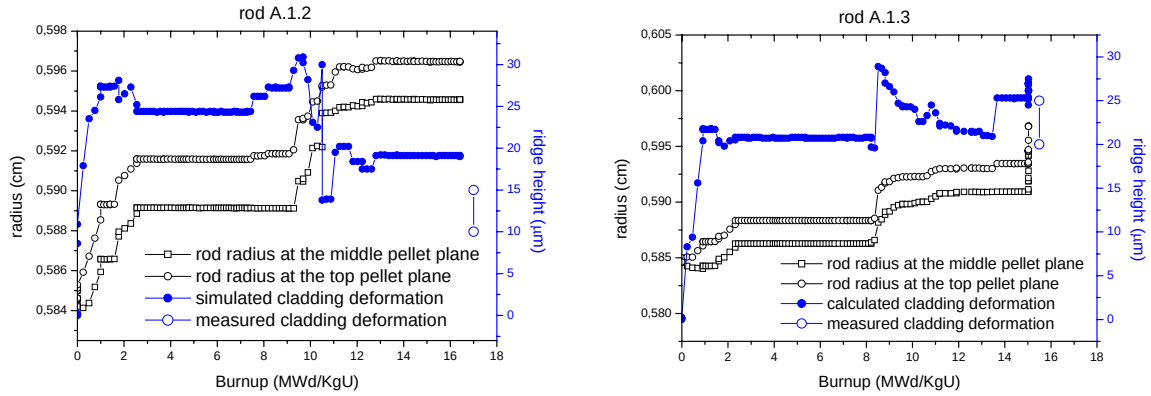

Figure 6: Evolution with burnup of the rod radius at the top and middle plane and difference between them for rods A.1.2 and A.1.3

The more remarkable feature evidenced in the postirradiation examinations is the presence of ridges on the external surface of the cladding accompanying the pellets distribution. Figure 6 shows the evolution with burnup of the radii of two rod sections, one taken at the middle and the other at the top of the pellet. The difference between them reveals the ridge effect. Given the large uncertainties of the experimental results only a range of values of ridge height is reported in [28]. The calculated results agree quite well with the measurements.

The evolution of the external pellet and internal cladding radii with burnup are represented in Figure 7 by the solid and dotted lines, respectively, obeying the left hand side scale. On the right hand side the hoop stress is plotted. The instants when pellet-cladding contact is produced can be recognized by the coincidence of the solid and dotted lines. This is accompanied by a change of sign of the hoop stress revealing the appearance of a traction stress on the cladding. The predicted final gap width falls within the range of the experimental values, between 8-12μm.

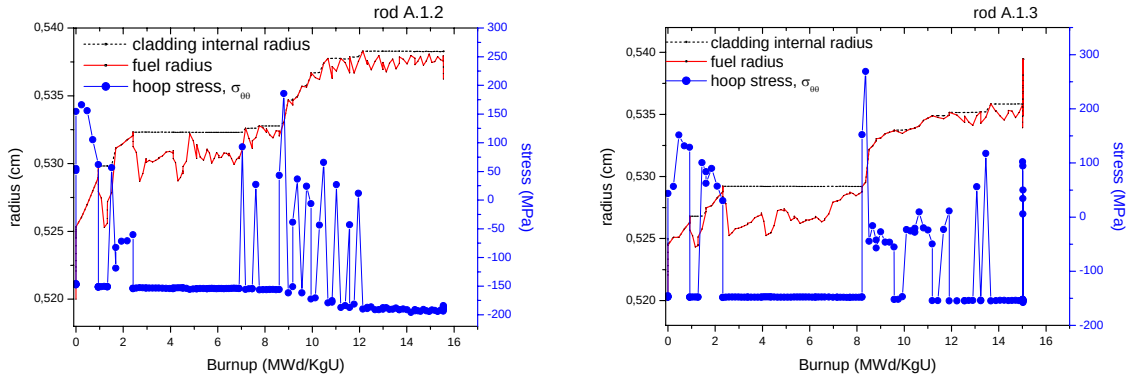

Figure7: Evolution with burnup of contact surface and hoop stress for rods A.1.2 and A.1.3

The CONTACT Experiment

The CONTACT series of experiments used short rods of Zry-4 clad - UO_2 pellets of typical PWR fuels that were irradiated in a pressurized water loop at a nearly constant power [29,30,31]. The CONTACT 1 rod was irradiated at a power level close to 40 kW/m and reached a discharge burnup of ~22 MWd/kgU; the internal pressure was 1 MPa of He. In CONTACT 2 the irradiation was performed at a power of 25 kW/m; the internal pressure was 0.1-0.2 MPa of He. At an early burnup of ~5.5 MWd/kgU a failure was detected, the rod was discharged and replaced with the rod CONTACT 2bis of identical design that reached a burnup of 12.4 MWd/kgU.

Figure 8 shows the centre temperature for CONTACT 1 and 2bis. A good prediction is obtained with DIONISIO in both cases. The comparison between the measured and simulated fission gas release for both experiments is shown in Figure 9. The EOL value for CONTACT 1 (18 %) is much higher than that for CONTACT 2bis (0.6%). The more demanding thermal conditions of experiment CONTACT 1 is responsible for this effect and also for the larger final clad deformation due to PCMI as compared with CONTACT 2bis, as can be seen in Figure 10 where the experimental data and the predictions of DIONISIO are shown. Both experiments were instrumented with thermocouples for which reason a central hole was made in the fuel pellets. The quite large diametral contraction observed is probably due to fuel relocation until it collapses onto the thermocouple wire [29]. This process is not simulated by DIONISIO because of lack of information and this is probably the cause of the departure between the simulated and measured values. Nevertheless, the general trend is correctly reproduced by DIONISIO, particularly for the large values of burnup, when the effect of hole closure starts to be less important as compared with the rest of the phenomena involved, which are accounted for by the code.

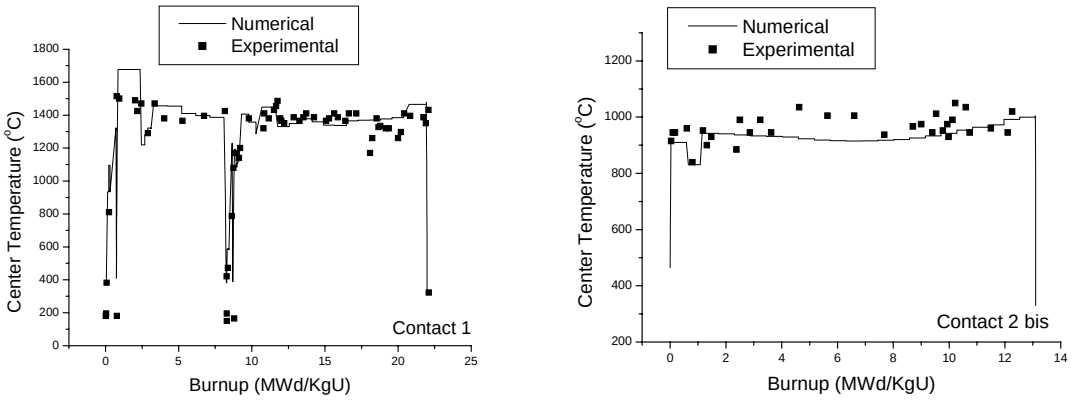

Figure 8: Temperature vs. burnup for CONTACT1 and CONTACT2 bis

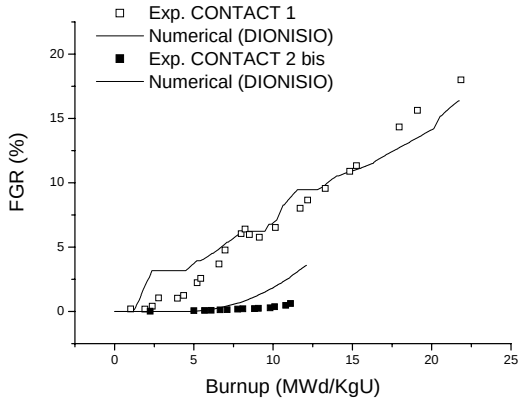

Figure 9: FGR vs. burnup for CONTACT1 and CONTACT 2 bis.

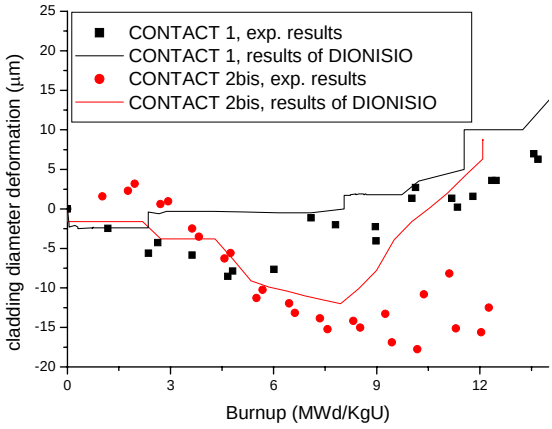

Figure 10: Cladding deformation for CONTACT 1 and 2bis.

Figure 11 shows the internal cladding and pellet radii vs. burnup, together with the hoop stress. Like in the MOX experiments, positive values of the hoop stress are obtained when pellet and cladding make contact. Its magnitude is smaller in the PWR than in the PHWR fuels due to the less demanding mechanical conditions.

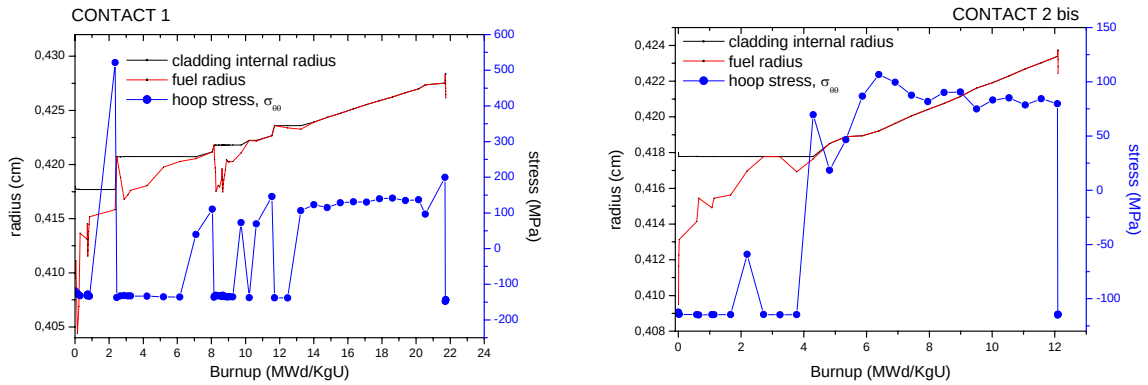

Figure 11: Evolution with burnup of contact surface and hoop stress for CONTACT 1 and 2bis

AECL Bundles JC and NR

The prototypes NR and JC were both 37-element fuel bundles for CANDU PHWR. Bundle NR was for the CANDU6 reactor and bundle JC for the Bruce-A Ontario Hydro reactors [32]. Both bundles were irradiated in the NRU experimental reactor at Chalk River Laboratories, in experimental loop facilities under typical CANDU reactor conditions of 9 to 10.5 MPa and 300°C, except that light water was used as coolant. The enrichment of the UO_2 fuel was 1.55 and 1.44 wt% U^{235} for the JC and NR bundles, respectively; the cladding material was Zircaloy-4. The JC rods contained 90% Ar and 10% He as filling gas mixture at 1 atm of internal pressure. For the case of NR, three different rod designs were used: NR1 with no plenum, NR2 with a plenum of 8 mm (0.35 cm^3) and NR3 with a 12mm plenum (0.58 cm^3). No element instrumentation was used during the irradiation but all the rods were subjected to extensive post-irradiation examination (PIE) that comprised dimensional changes, fission gas release, fuel burnup analysis and metallographic observations and grain size measurement. These experiments were simulated with DIONISIO. The numerical predictions and the PIE results are compared in Table III. The agreement is good in general although a slight tendency of DIONISIO to overestimating deformations is recognized.

Table III. Numerical predictions vs. PIE measurements for the AECL bundles JR and NR.

	JC		NC	
	Exp.	Num.	Exp.	Num.
FGR (cm^3)	48.3-60.6	42.52	39.1-42.6	34.15
FGR % Xe Kr He Ar	0.8595 0.0753 0.0413 0.0193	0.8471 0.0941 0.0058 0.0528	0.8467 0.1 0.0479 -	0.8413 0.0934 0.0651 -
ridge height (μm)	53-100	84	30-60	64
final diameter(mm)	1.314-1.320	1.321- 1.338	1.309-1.314	1.329-1.341
%strain, mid plane	0.32-0.69	0.86	0.36-0.90	2.31
%strain, ridge	1.16-2.1	2.15	(-)0.18-0.12	1.43
%length increm.	0.083-0.24	0.97	0.055-0.095	0.27
grain size (μm) external middle central	 8.5 29.75 CG (0.47)	 10 32.5 CG (0.56)	 - - CG (0.435)	 10 24.5 CG (0.56)

Experimental Fuel Elements (EFE) N° 89 and N° 51

These experiments [33] were performed in the Nuclear Research Institute Pitesti, Romania with the objective of getting information about the behavior of CANDU fuel elements within the limits of the design parameters. Two rods with different plenum sizes, instrumented with pressure transducers, were tested in the C2 irradiation device designed for the TRIGA reactor (14MW). The pellets of the EFE N°89 element had a density of 10,54 - 10,62g/cm^3, a diametral gap of 0.084 mm and an enrichment of 3,92wt%. For the EFE N°51 element, the values were 10.70 - 10.75g/cm^3, 0.100 - 0.130mm and 7,04wt%, respectively.

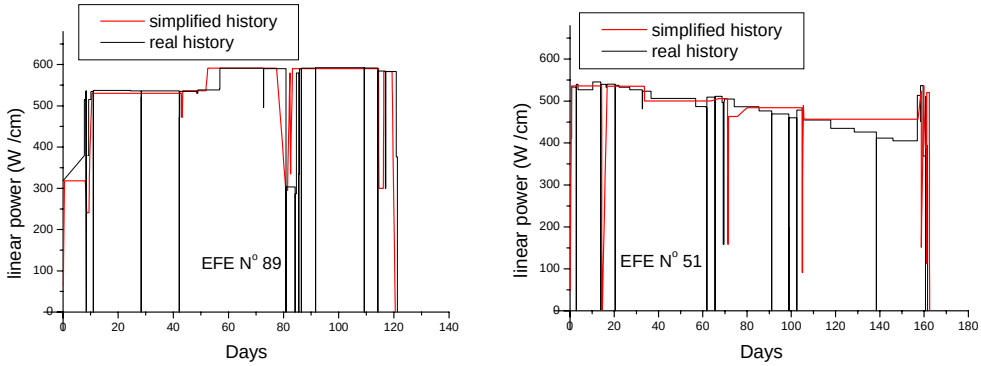

Figure 12: Real and simplified power histories of experiments N°89 and N°51.

The linear power was in the range 550±30W/cm during most of the irradiation for both experiments with the sole exception of the abrupt fluctuations at EOL in EFE N°51. The final burnup was 137.6 MWh/kgU for N°89 and 159.3 MWh/kgU for N°51. The coolant pressure was 10.7MPa for both experiments; the pH was in the range 9.5-10.5 for N°89 and 6.2-6.8 for N°51. Figure 12 shows the experimental power histories superimposed with the simplified versions used in DIONISIO.

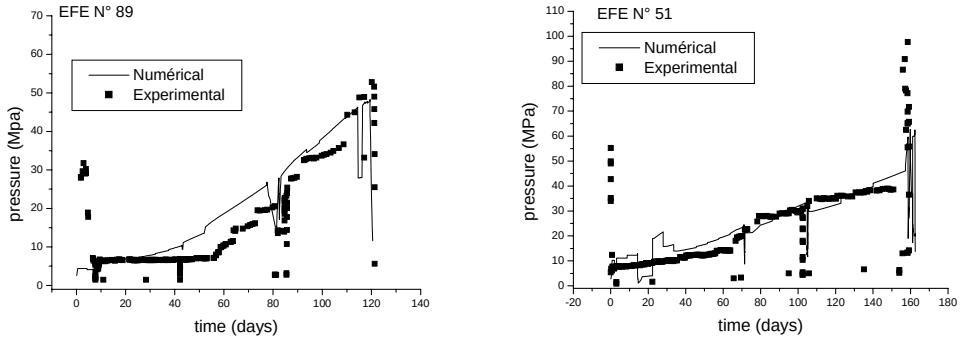

Figure 13: Comparison between the predictions of DIONISIO and the experimental values of pressure for the EFE N°89 and EFE N°51 elements.

Figure 13 shows the comparison between the predicted and experimental values of pressure. The agreement is good for EFE N°89 and also for EFE N°51 along most of the irradiation. A significant pressure increase is experimentally observed at the end of the latter experiment, when abrupt power scrams took place. It is generally accepted that sudden power variations produce micro-cracking in the pellet and in consequence a significant amount of gas is released [33]. This phenomenon is not modeled in DIONISIO yet and this is the reason why the predicted pressure at the end of the EFE N°51 experiment is below the measured value.

The measured volume of gas produced in the element EFE N°89 was 10.79cm^3; the prediction of DIONISIO is somewhat higher: 14.1cm^3. Some over prediction is also encountered for the void volume at EOF: the measured and calculated values are 1.22cm^3 and 1.88cm^3, respectively. For this reason the calculated internal pressure at EOL is slightly lower than that obtained in the experiment.

The temperature in the EFE N°89 experiment is higher than in EFE N°51 due, in the one hand, to the higher linear power and on the other hand to the higher pH of the coolant that promotes the formation of a thicker oxide layer.

FUMEX II

Several cases belonging to the FUMEX II exercise were reproduced with DIONISIO. A few of them are presented here to show the different abilities of the code and its limitations.

Ideal case 27-3a

Several ideal cases were proposed in the FUMEX II exercise to compare the performance of the participant codes. In particular, the case 27-3a, dedicated to CANDU fuel type elements, consist of eleven constant linear power histories between 100 – 600 W/cm up to a final burnup of 800 MWh/KgU (33.33 MWd/KgU).

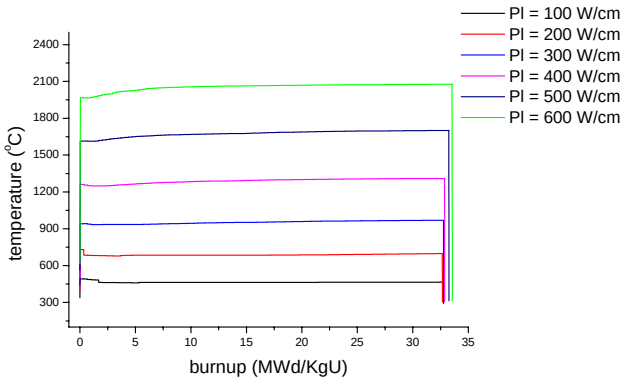

Figure 14: Centre temperature simulated with DIONISIO for the case 27-3a of FUMEX II

The simulations with DIONISIO of centre temperature, FGR, internal pressure, gaseous conductance in the gap and gap thickness during the irradiation time are shown in Figures 14

– 17, respectively. The typical evolution of the gap in CANDU fuels, i.e., closure shortly after irradiation initiation and permanence in this condition up EOL, is correctly predicted by DIONISIO, as shown in Figure 18.

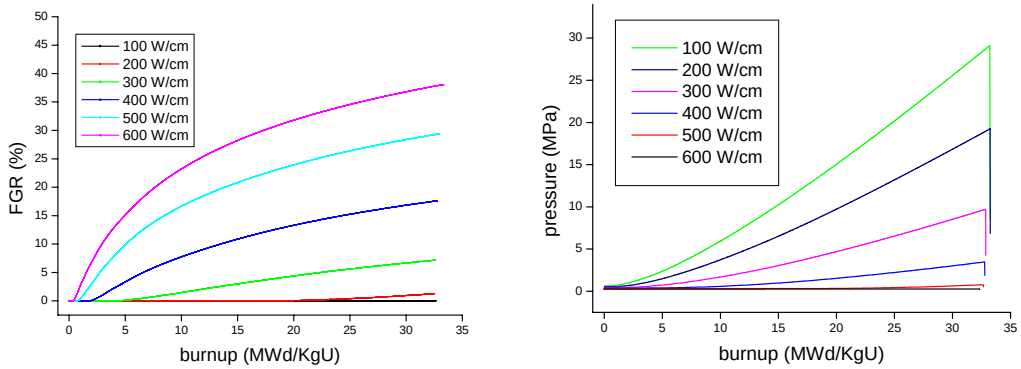

Figure 15: FGR and internal pressure simulated with DIONISIO for the case 27-3a of FUMEX II.

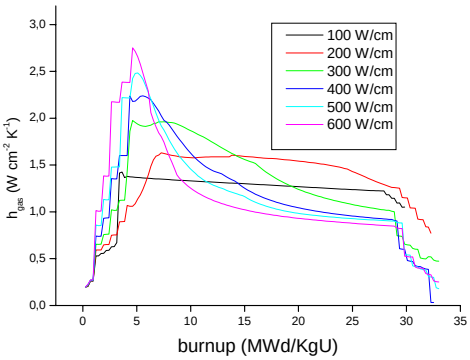

Figure 17: Gap gaseous conductance simulated with DIONISIO for the case 27-3a of FUMEX II

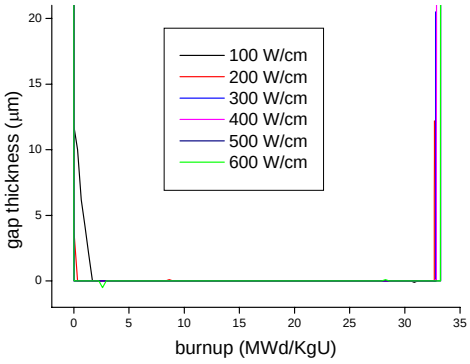

Figure 18: Gap size during the irradiation time simulated with DIONISIO for the case 27-3a of FUMEX II.

Transient thermal answer: IFA-507 experiment

This experiment [34,35], performed in the Halden Reactor in 1984, had the purpose of analyzing the thermal response of a fuel rod to a power ramp of a few seconds. The rods consisted of UO_2 pellets, with an enrichment of 10 % U^{235}, cladded in Zry-2. Two rods, designated TF3 and TF5, were equipped with thermocouples inserted at the centerline at a depth of 120 mm. At the time of the experiment the burn-up of these rods was ~18 $MWd/kgUO_2$ and the reactor was working at a power of ~15 MW. By the sudden removal of a shielding, the power was increased from 114 to 226 W/cm for TF3 rod and from 108 to 216 W/cm for TF5, resulting in a high ramp rate (~ 224 W/cm per minute)

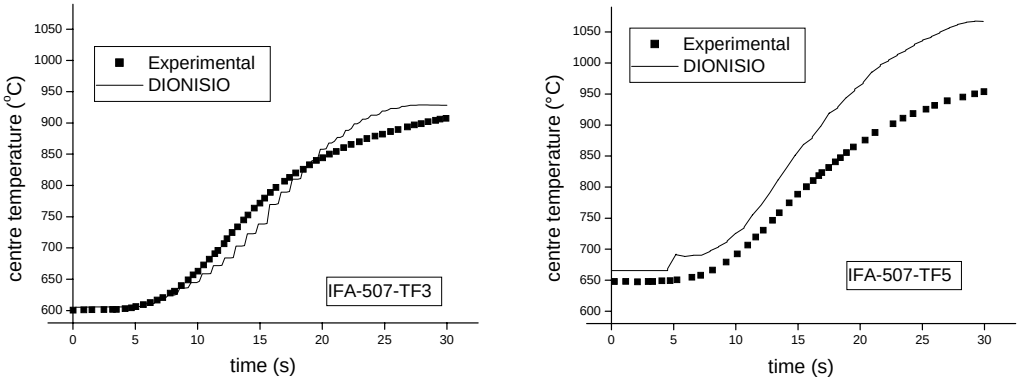

Figure 19: Centre temperature vs. transient time for the for TF3 and TF5 rods.

Figure 19 shows the comparisons between the predicted and experimental values of the centre temperature. The agreement can be considered good, taking into account the high velocities of the ramps and the short duration of the experiments (~30 sec.).

REGATE L10 experiment.

The REGATE experiment [36] was designed to study of the FGR and the diametral change of the rod due to fuel swelling during a power transient. A base irradiation was performed in a PWR during about 1139 days up to a burnup of 47 MWd/kgU. Then the rod was re-irradiated in the experimental reactor SILOE (Grenoble, France) where a fast power ramp of 10 W/cm/min was applied until reaching a linear power of 338 W/cm, and maintained at the high power level during 1.5 hours up to a total irradiation time of 1152 days. The PIE consisted of rod puncturing to determine FGR, measurement of diameter and oxide layer thickness, ceramography and determinations by EPMA of the radial profile of U and fission products at the location of the maximum power. Although DIONISIO does not contain adequate models to describe fast power ramps and high burnup, the example was run with the code to make evident its deficiencies and start the study to improve it.

Table IV shows the comparison between the experimental results and those predicted by DIONISIO. The most significant difference is in the FGR prediction, and hence the

corresponding model should be first replaced if the code is to be applied to simulate fast ramps and high burnups.

Table IV. Experimental results and predictions of DIONISIO for the REGATE L10 experiment

	experim.	DIONISIO
burnup at max. power level (MWd/kgM)	51	50.1758
FGR (%) before SILOE irradiation after SILOE irradiation	1.5 10.2	4.6 4.8
oxide layer thickness at max. power (μm)	28.6	21.6
external diameter at max. power before SILOE irradiation after SILOE irradiation	 0.9459 0.9515	 0.9571 0.9577
Xe retained in the pellets at max. power (wt%)	0.0 a 0.9	0.0018 -- 0.0391

RISO project, AN4 Test

The Riso National Laboratory in Denmark carried out three irradiation programs of slow ramp and hold tests [37,38], so called 'bump tests' to investigate fission gas release and fuel micro structural changes. In the third and final project, which took place between 1986 and 1990, the fuel was re-instrumented with pressure transducers and centerline thermocouples. The technique employed for re-fabrication involved freezing the fuel rod to hold the fuel fragments in position before cutting and drilling away the center part of the solid pellets to accommodate the new thermocouple.

The fuel used in the project was from: IFA-161 irradiated in the Halden BWR up to a burnup of 13 to 46 MWd/kgUO_2, GE BWR fuel irradiated in Quad Cities 1 and Millstone up to a burnup of 120 to 40 MWd/kgUO_2 and ANF PWR fuel irradiated in Biblis A up to a burnup of 38 MWd/kgUO_2. The data from the project are particularly valuable because of the in-pile data on fuel temperatures and pressures as well as extensive PIE. The final re-irradiation step of AN4 rod lasted 72 hours.

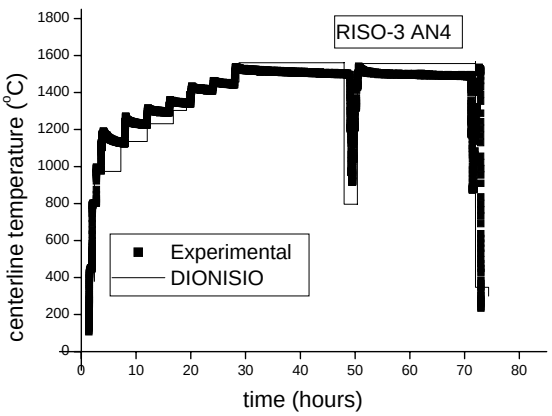

Figure 20: Centerline temperature vs. time for the AN4 rod.

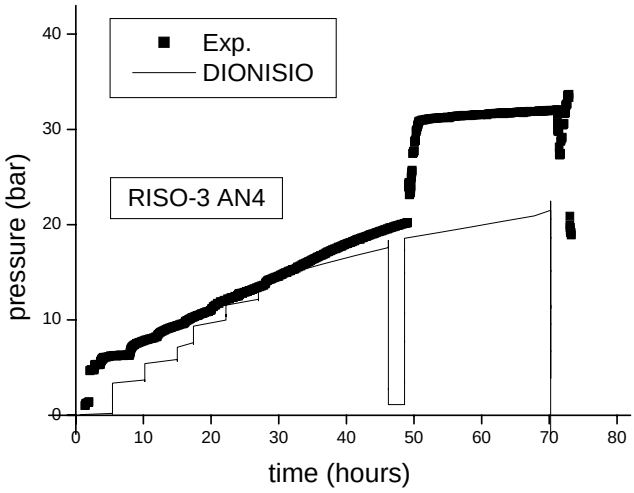

Figure 21: Internal pressure vs. time for AN4.

Figure 20 reveals the good quality of the thermal prediction. Nevertheless, the pressure is underpredicted by the code, as can be seen in Figure 21, due to the inadequacy of the gas release model in the burnup range involved, as already observed in the previous example.

OSIRIS experiment

The OSIRIS experiment [39] was performed with three standard PWR rods and one segmented rod irradiated in EDF commercial reactors. In this section the results of DIONISIO corresponding to one of these instrumented rods are presented and compared to the post-irradiation data. This example is intended to show a different use of the code. For the G07 rod, which is 380 cm long, the experiment provides the external temperature of the rod and the power history for 18 different axial sections. With these data 18 input files for the code are constructed and a detailed description of the whole rod is obtained. The 19th run contains an average power history with which the global physical parameters of the rod are evaluated. These results are presented in Table V.

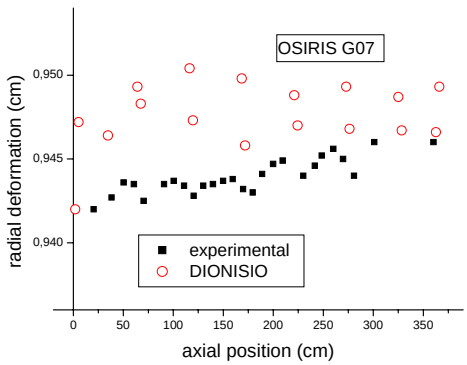

Figure 22: Radial deformation vs. axial position of the G07rod.

Table V. Average experimental results and predictions of DIONISIO for OSIRIS, G07 rod.

	experimental.	DIONISIO
burnup (MWd/KgU)	38.67	37.73
final gas volume (cm^3)	438.8	438
He (%)	0.977	0.99
Xe (%)	0.020	0.0018
Kr (%)	0.0021	0.0002
FGR (%)	0.49	0.1
internal pressure (bar)	35.7	59
internal free volume (cc)	12.3	15.59
H content in the rod (ppm)	350	203
oxide layer thickness (μm)	29	18.3
final gap size(μm)	11	10.5

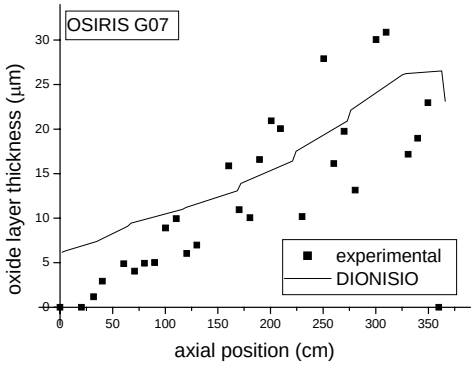

Figure 23: Oxide layer vs. axial position for the G07 rod of the OSIRIS experiment.

Figure 22 shows the measured and calculated radial deformation of the cladding. A certain overestimation of the strain in the first part of the rod is observed. In Figure 23 the oxide layer thickness measured along the rod and that predicted by DIONISIO are represented. The agreement fairly good.

5. Discussion

Simulation of PCMI is a complex task not only because of the numerical difficulties involved but also because it is connected with the rest of the physical and chemical phenomena that take place within the rod. In particular, the quality of the thermal predictions is determinant of the accuracy of the whole simulation.

The model of thermal conductance of the gap included in DIONISIO considers the contributions of radiation, conduction through the gas mixture and the solid-solid contact spots between rough surfaces. A correction term for low gas pressures is also included. The

models and parameters involved in these descriptions were taken from the literature, except for the latter which was developed by this working group.

The model of mechanical contact included in DIONISIO allowed an acceptable description of the bamboo effect and the radial cladding deformation in all the cases tested.

Each algorithm was separately tested and successfully compared with data available in the literature. With these models included in DIONISIO, the code was applied to the simulation of irradiation experiments of rods of diverse characteristics. The agreement with the measured values is satisfactory, revealing the accuracy of the individual models and the adequate coupling among them.

A limitation of DIONISIO is recognized in the high burnup range since no specific models representing micro-cracking are included up to now. This phenomenon is presumed to be responsible for the gas release enhancement experimentally observed in that period even under stationary irradiation conditions.

Acknowledgments

The authors are indebted to NEA Data Bank for the provision of the experimental results and to Ana María Lerner, who made the necessary arrangements for obtaining the data.

Bibliography

[1] L.Caillot, B.Linet, C.Lemaignan, *Pellet clad interaction in PWR fuel. Analytical irradiation experiment and finite element modelling*, Proc. SMIRT 12, Stuttgart, Germany, 1993.
[2] J.Mathews, *The quantitative description of deformation and stress in cylindrical fast reactor fuel pins*, in Advances in Nuclear Science and Technology, Vol.6 (1972), Academic Press.
[3] A.Denis, R.Piotrkowski, *Simulation of isothermal fission gas release*, J.Nucl. Mater. 229 (1996) 149–154.
[4] A.Denis, R.Piotrkowski, *A fission gas release model*, Water Reactor Fuel Element Modeling at High Burnup and Experimental Support, IAEA-TECDOC-957, (1997) 455–465.
[5] D.R.Olander, *Thermodynamics and transport processes in reactor fuel*. Pure & Appl. Chem., Vol. 67, No. 6 (1995) 1003-1010.
[6] F.Nagase, T. Otomo, H.Uetsuka, *Oxidation kinetics of low-Sn Zircaloy-4 at the temperature range from 773 to 1573K*, Vol. 40, No. 4, (April 2003) p. 213–219.
[7] L.J.Segerlind, *Applied finite element analysis*, 2nd Ed., Wiley (1984).
[8] *Handbook of materials properties for use in the analysis of light water reactor fuel behavior*, MATPRO version 11, NUREG/CR-0497, TREE–1280 (1979).
[9] D.R.Olander, *Fundamental Aspects of Nuclear Reactor Fuel Elements*, Technical Information Center, 1976.
[10] Kinoshita and Ichikawa, *Analysis of fuel rod deformation*, Nucl. Eng. and Des. 56 (1980) 49-56.
[11] J.K.Fink, L.Leibowitz, *Thermal conductivity of zirconium,* J.Nucl. Mater. 226 (1995) 44-50.
[12] G.Delete, M.Charles, *Thermal conductivity of fully dense unirradiated UO_2: a new formulation from experimental results between 100°C and 2500°C and associated fundamental properties*, Water Reactor Fuel Element Modelling at High Burnup and its Experimental Support, IAEA–TECDOC–957, IAEA (1997) 203–216.
[13] A.Levy, B.Pifko, *On computational strategies for problems involving plasticity and creep*, International Journal for Numerical Methods in Engineering, Vol. 17 (1981) 747-771.
[14] Berna G.A et al., *FRAPCON-2: A computer code for the calculation of steady state thermal-mechanical behavior of oxide fuel rods*, NUREG/CR-1845 (1980)
[15] A.Marino, E.Savino, S.Harriague, *BACO code version 2.20: a thermomechanical description of a*

nuclear fuel rod, J.Nucl. Mater. 229 (1996) 155–168.
[16] A.Soba, A.Denis, *Simulation with DIONISIO 1.0 of Thermal and Mechanical Pellet-Cladding Interaction in Nuclear Fuel Rods*, J.Nucl. Mater. (in press)
[17] A.Soba, *Comparación entre modelos de conductancia térmica de contacto UO_2-Zircaloy,* MECON 2005.
[18] S.Wahid, C.Madhusudana, *Gap conductance in contact heat transfer*, International Journal of Heat Transfer 43 (2000) 4483-4487
[19] L.Tong, J.Weisman, *Thermal analysis of pressurized water reactors*, American Nuclear Society, La Grange Park, Illinois, USA (1995).
[20] J.Ainscough, *Gap conductance in Zircaloy-clad LWR fuel rods*, OECD, NEA, (April 1982).
[21] G.Jacobs, N.Todreas N, Nucl. Sci. and Eng. 50 (1973) 283-290.
[22] F.J.Gallego, J.J. Anza, *Un modelo de elementos finitos mixtos para la resolución del problema del contacto elástico*, Métodos Numéricos para Cálculo y Diseño en Ingeniería, vol5, 2, 163-184 (1989)
[23] U.Sellgren, S.Björklund, S.Andersson, *A finite element-based model of normal contact between rough surfaces*, Wear 254 (2003) 1180,1188
[24] J. Zurita, M. Doblare y L. García, *Determinación de tensiones de contacto mediante el M.E.C. en problema multicuerpo con simetría axial*, Métodos Numéricos para Cálculo y Diseño en Ingeniería, Vol. 9, 1 (1993) 15-34
[25] K.Bathe, A.Chaudhary, *A solution method for planar and axisymmetric contact problems*, Int. J. Num. Meth. Engng 21 (1985) 65-88.
[26] K.Bathe, *Finite Element Procedures*, Prentice Hall, 1996.
[27] *Fuel Modeling at extended burnup*, IAEA–TECDOC–998, IAEA (1998).
[28] A.Marino, E.Pérez, P.Adelfang, *Irradiation of Argentine (U,Pu)O_2 -MOx fuels. Postirradiation results and experimental analysis with the BACO code*, J.Nucl. Mater. 229 (1996) 169-186
[29] IFPE/CONTACT Rev.1. Database for CONTACT experiments irradiated at CEA Grenoble, J.A Turnbull, October 1998.
[30] M.Bruet, J.Dodalier, P.Melin, M.Pointud: *CONTACT 1 and 2 experiments: behaviour of PWR fuel rods up to 15000 MWd/TU*, IAEA Specialists' Meeting on Water Reactor Fuel Elements Performance Computer Modelling, Blackpool, UK, March 1980.
[31] M.Charles, C.Lemaignan, *Fuel performance under normal PWR conditions: a review of relevant experimental results and models*, J. Nucl. Mater. 188 (1992) 96-103.
[32] V.Arimescu, NEA-1596 IFPE/AECL-BUNDLE, Chalk River, Ontario, Canada, Feb. 2000.
[33] C.Paraschiv, *IAEA/OECD-NEA Fuel performance Database*, May 2001.
[34] IFPE/IFA-507-TF3-TF5. NEA-1729/01. Oct. 2004.
[35] E.Kolstad, *A Study of the Thermal Behaviour of LWR Fuel Designs under Transient Power Conditions,* HWR-120, April 1984.
[36] J.A.Turnbull, *FGR and fuel swelling during power transient at medium burn-up (SILOE reactor)*, NEA-1696 IFPE/REGATE L10.3, CEA, Cadarache, April 2004.
[37]*Fuel Performance Data from 3rd Risoe Fission Gas Release,* NEA-1493, IFPE/RISOE-III, Risoe National Laboratory, Denmark, Oct.1995.
[38] *The third RISO fission gas project. Bump test AN4 (CB7-2R)*, REP-FGP3-AN4, RISO Materials Department, Sept. 1990.
[39]DATABASE FOR EDF/FRAMATOME/CEA PWR FUEL RODS. Report FF06E2BV/G07/1067. Revised by J. A. Turnbull, 21 January, 2003